





Article

The Isotopic Characteristics, Sources, and Formation Pathways of Atmospheric Sulfate and Nitrate in the South China Sea

Yongyun Zhang¹, Min Gao¹, Xi Sun^{1,2}, Baoling Liang^{1,3}, Cuizhi Sun¹, Qibin Sun^{1,4}, Xue Ni^{1,5}, Hengjia Ou¹, Shixin Mai¹, Shengzhen Zhou^{1,6,7,*} and Jun Zhao^{1,6,7}

- ¹ Guangdong Province Key Laboratory for Climate Change and Natural Disaster Studies, and Southern Marine Science and Engineering Guangdong Laboratory (Zhuhai), School of Atmospheric Sciences, Sun Yat-Sen University, Zhuhai 519082, China; zhangyy385@mail2.sysu.edu.cn (Y.Z.); gaom39@mail2.sysu.edu.cn (M.G.); 13281849402@163.com (X.S.); liangbl3@mail3.sysu.edu.cn (B.L.); suncuizhi@sml-zhuhai.cn (C.S.); sunqb@mail3.sysu.edu.cn (Q.S.); nixue@mail2.sysu.edu.cn (X.N.); ouhj@mail2.sysu.edu.cn (H.O.); maishx3@mail2.sysu.edu.cn (S.M.); zhaojun23@mail.sysu.edu.cn (J.Z.)
- ² Centre for Isotope Research (CIO), Energy and Sustainability Research Institute Groningen (ESRIG), Faculty of Science and Engineering (FSE), University of Groningen, 9747 AG Groningen, The Netherlands
- ³ Guangzhou Sub-Branch of Guangdong Ecological and Environmental Monitoring Center, Guangzhou 510006, China
- ⁴ Dongguan Meteorological Bureau, Dongguan Engineering Technology Research Center of Urban Eco-Environmental Meteorology, Dongguan 523086, China
- ⁵ Guangzhou Climate and Agrometeorology Center, Guangzhou 511430, China
- ⁶ Guangdong Provincial Observation and Research Station for Climate Environment and Air Quality Change in the Pearl River Estuary, Zhuhai 519082, China
- ⁷ Key Laboratory of Tropical Atmosphere-Ocean System, Ministry of Education, Zhuhai 519082, China
- * Correspondence: zhoushz3@mail.sysu.edu.cn

Abstract: The South China Sea (SCS) is a crucial region for studying atmospheric aerosols, given its unique geographical location and the interaction of various natural and anthropogenic sources. In this study, we measured the isotopic characteristics of sulfate and nitrate in PM_{2.5} and utilized a Bayesian isotope mixing model (SIAR) to analyze their sources and formation pathways. Sulfur isotopic values in sulfate ($\delta^{34}\text{S-SO}_4^{2-}$) were $8.7 \pm 1.8\text{‰}$, while nitrogen and oxygen isotopic values in nitrate ($\delta^{15}\text{N-NO}_3^-$ and $\delta^{18}\text{O-NO}_3^-$) were $-0.9 \pm 2.4\text{‰}$ and $52.3 \pm 7.3\text{‰}$, respectively. The results revealed that sulfate was primarily influenced by marine biogenic sulfur emissions (mostly dimethyl sulfide, DMS), fossil fuel combustion, and biomass burning. Nitrate formation was dominated by the $\text{NO}_2 + \bullet\text{OH}$ pathway (accounting for 69.8–85.7%), with significant contributions from vehicle emissions, biomass burning, and lightning. These findings offer key insights into the complex interactions between natural and anthropogenic aerosol sources in the SCS, contributing to a broader understanding of marine aerosol chemistry.

Keywords: PM_{2.5}; nitrate isotopes; sulfate isotopes; source apportionment; formation pathways; South China Sea



Citation: Zhang, Y.; Gao, M.; Sun, X.; Liang, B.; Sun, C.; Sun, Q.; Ni, X.; Ou, H.; Mai, S.; Zhou, S.; et al. The Isotopic Characteristics, Sources, and Formation Pathways of Atmospheric Sulfate and Nitrate in the South China Sea. *Sustainability* **2024**, *16*, 8733. <https://doi.org/10.3390/su16208733>

Academic Editor: Joana Ferreira

Received: 27 August 2024

Revised: 1 October 2024

Accepted: 5 October 2024

Published: 10 October 2024



Copyright: © 2024 by the authors. Licensee MDPI, Basel, Switzerland. This article is an open access article distributed under the terms and conditions of the Creative Commons Attribution (CC BY) license (<https://creativecommons.org/licenses/by/4.0/>).

1. Introduction

Aerosols or particulate matter (PM) can potentially influence global atmospheric processes, atmospheric radiation, climate, and ecosystem balance and can even pose risks to human health through pollution [1–3]. Therefore, understanding the composition, sources, and formation pathways of atmospheric aerosols is crucial for developing effective mitigation strategies. The South China Sea (SCS), located south of mainland China, is part of the Northwest Pacific and one of the largest marginal seas in the world. It is surrounded by many islands and land masses (Figure 1). As a result, the SCS receives large amounts of aerosols from neighboring regions via long-range atmospheric transport, while ship emissions and marine sources contribute to its complex atmospheric composition [4,5].

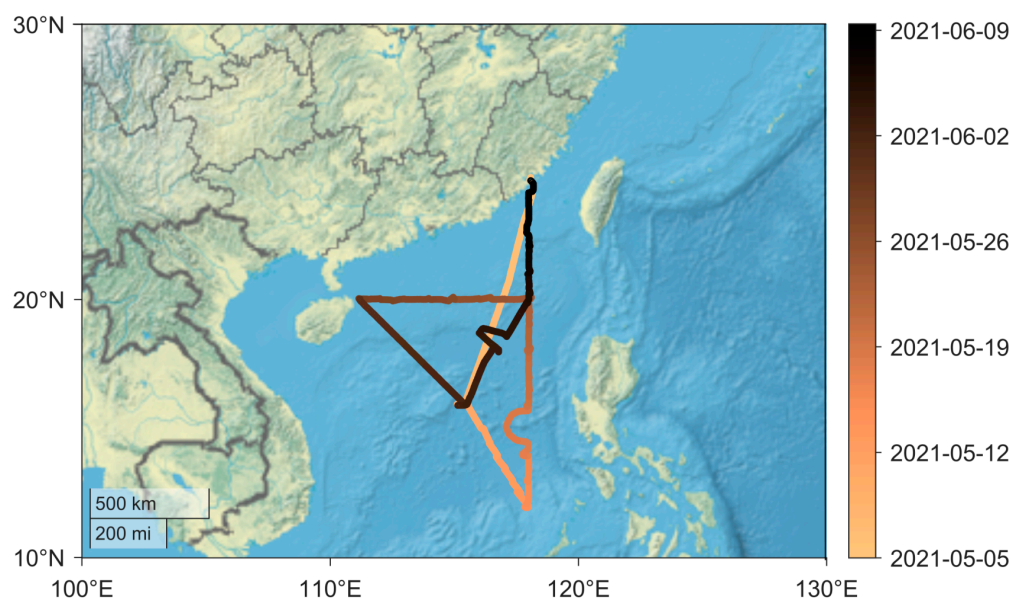


Figure 1. Cruise route during a campaign in the SCS from 5 May to 9 June 2021.

Water-soluble inorganic ions such as nitrate, sulfate, and ammonium constitute the main components of $PM_{2.5}$ (fine particulate matter) and play crucial roles in aerosol chemistry, cloud formation, and hazy weather conditions [1,6]. Nitrate and sulfate are secondary products formed through the oxidation of precursor gases, specifically nitrogen oxides and sulfur dioxide [7,8]. The isotopic compositions of nitrogen ($\delta^{15}N$) in nitrate and sulfur ($\delta^{34}S$) in sulfate serve as valuable proxies, providing critical information on the sources of nitrogen and sulfur gas emissions [7,9]. These proxies can be used to effectively differentiate between natural and anthropogenic sources [8]. Conversely, the oxygen isotopic compositions ($\delta^{18}O$ and $\delta^{17}O$) are linked to the incorporation of oxygen atoms from various atmospheric oxidants [7,10]. Nitrate formation in the atmosphere occurs through different mechanisms, including the reaction of NO_2 with hydroxyl radicals ($\bullet OH$), N_2O_5 with H_2O or Cl^- , and NO_3 with VOCs [11,12]. Each pathway imparts a distinct isotopic signature, enabling the identification of the primary nitrate formation mechanisms under various atmospheric conditions [11,12].

With the advances in isotope technology, numerous studies have been conducted on nitrate and sulfate isotopic signatures, sources, and formation mechanisms in polar regions, the open oceans, marginal seas, and inland urban areas [7,13–16]. Sulfur isotope values in sulfate (SO_4^{2-}) aerosols tend to be higher in the polar and open-ocean regions than in other regions, mainly driven by contributions from biogenic sulfur (mostly DMS) and sea salt, with $\delta^{34}S$ values of 18.9–20.3‰ [17] and 20.2–22.1‰ [18], respectively. In contrast, sulfate isotope values in inland urban areas are much lower and are primarily influenced by the oxidation of sulfur-containing compounds from anthropogenic activities, such as fossil fuel combustion and biomass burning, with $\delta^{34}S$ values of -2.88 – 10 ‰ [19–21] and 4.2–7.9‰ [20,22]. Nitrate aerosol concentrations and nitrogen isotopes tend to be higher in urban areas than in the open ocean, mainly due to the effects of anthropogenic activities such as vehicle exhaust, biomass burning, and coal combustion, with $\delta^{15}N$ values of -7 ± 4.8 ‰ [15], -1.7 ± 4.7 ‰ [23–25], and 18.6 ± 2.9 ‰ [26] respectively. However, aerosols in marginal seas often result from a combination of oceanic and terrestrial sources, making their isotopic characteristics and sources more complex. Compared to inland areas, there are still fewer observations of nitrate and sulfate isotopes in the SCS.

Therefore, to better explore the potential sources and contributions of aerosols in the SCS, this study comprehensively analyzed the composition of water-soluble inorganic ions in $PM_{2.5}$. By utilizing the isotope compositions of nitrogen and oxygen in nitrate, a Bayesian model was applied to trace the sources and formation pathways of nitrate. Similarly, the sulfur isotope composition of sulfate was analyzed using the model to

determine its potential source contributions. Additionally, this study also provides the first report of sulfur isotope compositions in PM_{2.5} from ship-based measurements in the SCS. These findings offer key insights into the complex interactions between natural and anthropogenic aerosol sources in the SCS, contributing to a broader understanding of marine aerosol chemistry. This information is critical for developing effective air quality management strategies and mitigating the impacts of air pollution on human health and the environment.

2. Materials and Methods

2.1. Study Area and Sample Collection

The cruise campaign was a routine comprehensive exercise organized by Sun Yat-sen University (SYSU) from 5 May to 9 June 2021, encompassing a variety of multidisciplinary sciences (i.e., atmospheric, oceanic, geological, and biological sciences). The vessel traveled across a wide geographic range in the SCS, from 12°00' to 24°33' N and 111°6' to 118°05' E (Figure 1). In contrast to previous island-based and shorter transit observations in the SCS, this study offers a more comprehensive representation.

Twenty-nine PM_{2.5} samples were collected from SCS during the study voyage. The sampling instrument was a high-volume air sampler (TE-6070, TISCH), with a sampling flow rate of 1.05 ± 0.03 m³/min. Each sample was collected for 23.5 to 48 h, and all samples were then stored in a -20 °C freezer until analysis. In this study, all sampling equipment was placed at the bow, away from the aft chimney, to minimize the ship's exhaust gases' interference with the data. Meteorological data such as temperature, relative humidity, wind speed, and wind direction were based on the observations from the shipborne meteorological station, located at the bow of the ship. During the campaign in Figure 2, predominantly influenced by the summer monsoon, the prevailing winds in the SCS were from easterly to southwesterly. During the summer, the SCS experienced temperatures of 29.4 ± 1.6 °C and relative humidity of $79.5 \pm 5.0\%$, characterized by a hot and humid environment.

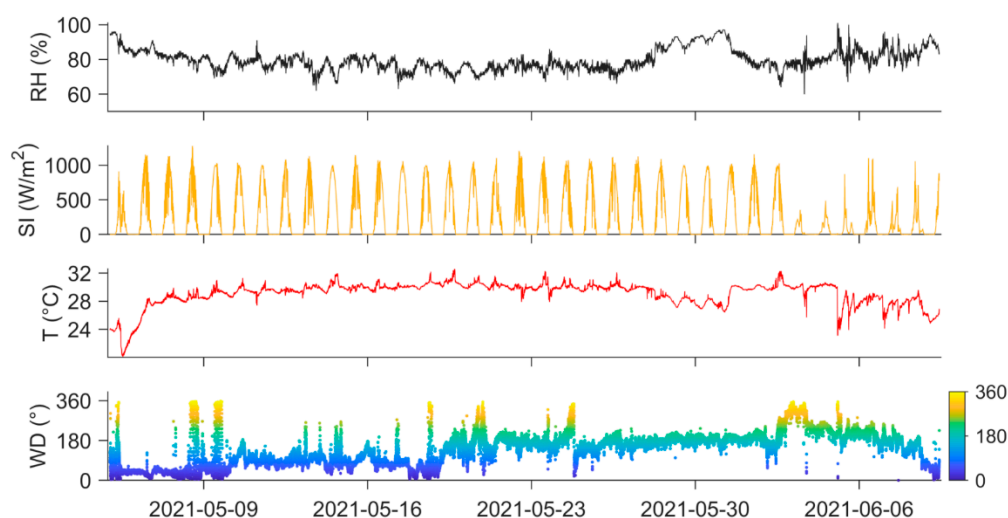


Figure 2. Time series of meteorological variables: relative humidity (RH), solar irradiance (SI), temperature (T), and wind direction (WD) during the campaign.

2.2. Ion and Isotope Determination

For ionic composition analysis, four circular filter membranes with an 8 mm radius were cut for each sample and loaded into centrifuge tubes. The following procedures were undertaken: 15 mL of Milli-Q water was added, followed by ultrasonication for 30 min. It was allowed to stand for 5 min and then filtered. The filtered solution was subsequently analyzed by ion chromatography (Dionex Aquion, Thermo Fisher Scientific (China) Co., Ltd., Shanghai, China.) for the concentration of major ion components (SO₄²⁻, Cl⁻, NO₃⁻, NH₄⁺, Ca²⁺, Na⁺, K⁺, Mg²⁺, and F⁻). Typically, the mass concentration of sea-salt sulfate

($ss\text{-SO}_4^{2-}$) was calculated as $ss\text{-SO}_4^{2-} = 0.252 * [\text{Na}^+]$, assuming that Na^+ was entirely derived from the sea salt contribution. The mass concentration of non-sea-salt sulfate ($nss\text{-SO}_4^{2-}$) was then determined by $nss\text{-SO}_4^{2-} = [\text{SO}_4^{2-}] - [ss\text{-SO}_4^{2-}]$ [19].

The values of $\delta^{15}\text{N}\text{-NO}_3^-$ and $\delta^{18}\text{O}\text{-NO}_3^-$ were determined by the denitrifier method [27,28]. This method is well established, and the detailed analysis process can be found in previous studies [9,10]. Here, only a brief overview of the procedure is given. Firstly, denitrifying bacteria (*Pseudomonas aureofaciens* (ATCC 13985)) were cultured. Secondly, 20 nmol NO_3^- was added to the denitrifying bacteria solution so that NO_3^- was completely converted to N_2O . Finally, a GasBench isotope ratio mass spectrometer (Delta V Advantage, Thermo Fisher Scientific, Waltham, MA, USA) was used to analyze $\delta^{15}\text{N}\text{-N}_2\text{O}$ and $\delta^{18}\text{O}\text{-N}_2\text{O}$. Four international reference standards (USGS32, USGS34, USGS35, and IAEA- NO_3^-) and one laboratory reference standard were used for the analytical calibration. The standard deviations of $\delta^{15}\text{N}\text{-NO}_3^-$ and $\delta^{18}\text{O}\text{-NO}_3^-$ were within $\pm 0.3\%$.

A method used in previous studies [29,30] was adopted for determining the value of $\delta^{34}\text{S}\text{-SO}_4^{2-}$. Briefly, an appropriate amount of sample was taken to ensure that 340–450 μg BaSO_4 powder would be produced from the reaction. The sample was then filtered and extracted into an aqueous solution. The filtrate was then acidified with an amount of HCl to a $\text{pH} < 2$, followed by addition of 3 mL 1 mol/L BaCl_2 solution, and it was allowed to react at room temperature for 24 h after full oscillation. The resulting BaSO_4 precipitate was subsequently filtered out, and the filtrate was checked with AgNO_3 solution to ensure no additional white precipitate was produced so that Cl^- interference could be excluded. Finally, the filter membrane with the BaSO_4 precipitate was placed in a muffle furnace at 800°C for 4 h to produce pure BaSO_4 precipitate. Once obtained, the BaSO_4 was then analyzed for the sulfur isotopic composition by combustion to SO_2 using an isotope ratio mass spectrometer (MAT253, Thermo Fisher Scientific, Waltham, Massachusetts, USA), based on a quantitative method called dynamic flash combustion [31]. IAEA SO-5 was used as the reference material for BaSO_4 ($\delta^{34}\text{S} = 0.5\%$).

The isotopic compositions are presented relative to reference standards, utilizing the delta (δ) notation, and are expressed in permil units ($\%$), as delineated in Equation (1):

$$\delta(\%) = 1000 \left(\frac{R_{\text{samp}}}{R_{\text{ref}}} - 1 \right) \quad (1)$$

The ratio R denotes the relative abundance of heavy to light isotopes, such as $^{15}\text{N}/^{14}\text{N}$, $^{34}\text{S}/^{32}\text{S}$, and $^{18}\text{O}/^{16}\text{O}$, for both the analyzed sample and the reference standards.

2.3. Source Apportionment Using the Bayesian Model

To apportion the sources of sulfate and nitrate as well as different HNO_3 formation pathways to nitrate in $\text{PM}_{2.5}$ of the SCS, a Bayesian isotope mixing model (Stable Isotope Analysis in R, SIAR, <https://rdrr.io/cran/siar/>, accessed on 6 June 2024) was employed [13,15,32]. The Bayesian approach provides a probabilistic framework that combines isotopic signatures with prior information about potential sources. The Bayesian isotope mixing model and its detailed description can be found in Parnell et al. (2013) [33]. The formulation of the Bayesian isotope mixing model for N -mixture measurements on J isotopes with k source contributors involves the following formulas:

$$Y_i \sim N(p_i^T (s_i + c_i), \Sigma) \quad (2)$$

$$S_{ik} \sim N(\mu_k^s, \Sigma_k^s) \quad (3)$$

$$C_{ik} \sim N(\mu_k^c, \Sigma_k^c) \quad (4)$$

$$\varepsilon_i \sim N(0, \Sigma) \quad (5)$$

where Y_i is the J -vector of the isotope values for mixture i , which represents the isotope measurement in mixture i for isotope j ; s_{ik} is the J -vector of the isotope source values for

mixture i on source k ; c_{ik} is the J -vector of the trophic enrichment factor values for mixture i on source k ; and ε_i is the J -vector of the residual terms for mixture i with a covariance matrix. The model also considered isotopic fractionation processes occurring during atmospheric transport and transformation. Markov chain Monte Carlo (MCMC) simulations were conducted to estimate the posterior distributions of source contributions, providing a comprehensive uncertainty analysis. The results of the Bayesian model included the proportional contributions of each source to the total sulfate and nitrate concentrations in the aerosol samples, along with credible intervals reflecting the uncertainties.

Drawing from previous studies [32,34], the relative contributions of HNO_3 generated by different pathways to nitrate in $\text{PM}_{2.5}$ were estimated using the SIAR model as follows:

$$[\delta^{18}\text{O} - \text{NO}_3^-] = \sum_1^4 f_{(n)} \times [\delta^{18}\text{O} - \text{HNO}_{3(n)}] \quad (6)$$

$$f_{(1)} + f_{(2)} + f_{(3)} + f_{(4)} = 1 \quad (7)$$

where $\delta^{18}\text{O}\text{-HNO}_{3(1)}$, $\delta^{18}\text{O}\text{-HNO}_{3(2)}$, $\delta^{18}\text{O}\text{-HNO}_{3(3)}$, and $\delta^{18}\text{O}\text{-HNO}_{3(4)}$ represent the $\delta^{18}\text{O}\text{-HNO}_3$ values produced by the $\text{NO}_2 + \bullet\text{OH}$, $\text{N}_2\text{O}_5 + \text{H}_2\text{O}$, $\text{NO}_3 + \text{VOCs}$, and $\text{N}_2\text{O}_5 + \text{Cl}^-$ pathways, respectively. The relative contributions of these pathways to nitrate in $\text{PM}_{2.5}$ are denoted as $f_{(1)}$, $f_{(2)}$, $f_{(3)}$, and $f_{(4)}$.

2.4. Complementary Analysis

To determine the origins and transport pathways of air masses reaching the SCS sampling sites, backward trajectories were calculated using the Hybrid Single-Particle Lagrangian Integrated Trajectory (HYSPLIT) model. The model was run using meteorological data from the National Oceanic and Atmospheric Administration (NOAA) Global Data Assimilation System (GDAS). The starting point of the trajectories was set at the midpoint of each sample cruise coordinate, and trajectories were computed for 72 h at an altitude level (500 m above ground level) to account for temporal variations in air mass transport. The backward trajectories helped to identify potential source regions and transport patterns, which were further analyzed to correlate with the isotopic signatures of sulfate and nitrate in the collected $\text{PM}_{2.5}$ samples.

In this study, SPSS (version 29) and Excel (version 2019) were used for data processing, while MATLAB (version R2022a), R (version 4.3.1), Origin (version 2021b), Surfer (version 26), Grapher (version 20), and MeteoInfo (version 3.8.11) were used for plotting.

3. Results and Discussion

3.1. Ion Component Characteristics and Stoichiometric Relationship

3.1.1. Ion Component Characteristics

The mean mass concentration of $\text{PM}_{2.5}$ water-soluble ions in the SCS during the warm season was $3.1 \pm 1.6 \mu\text{g}/\text{m}^3$. The main components were SO_4^{2-} ($1.8 \pm 0.9 \mu\text{g}/\text{m}^3$), Na^+ ($0.4 \pm 0.4 \mu\text{g}/\text{m}^3$), and NH_4^+ ($0.3 \pm 0.2 \mu\text{g}/\text{m}^3$) (Figure 3 and Table 1), accounting for 58.7%, 14.3%, and 10% of the total water-soluble ions, respectively. Notably, sulfate accounted for a significantly larger proportion than the other ions in terms of the mass concentration. The mass concentrations of Cl^- ($0.2 \pm 0.4 \mu\text{g}/\text{m}^3$) and NO_3^- ($0.2 \pm 0.4 \mu\text{g}/\text{m}^3$) in $\text{PM}_{2.5}$ accounted for 5.9% and 5.8%, respectively. The remaining ions, including Ca^{2+} , Mg^{2+} , and K^+ , had a cumulative mass concentration of $0.2 \pm 0.1 \mu\text{g}/\text{m}^3$, constituting the remaining 5.3%.

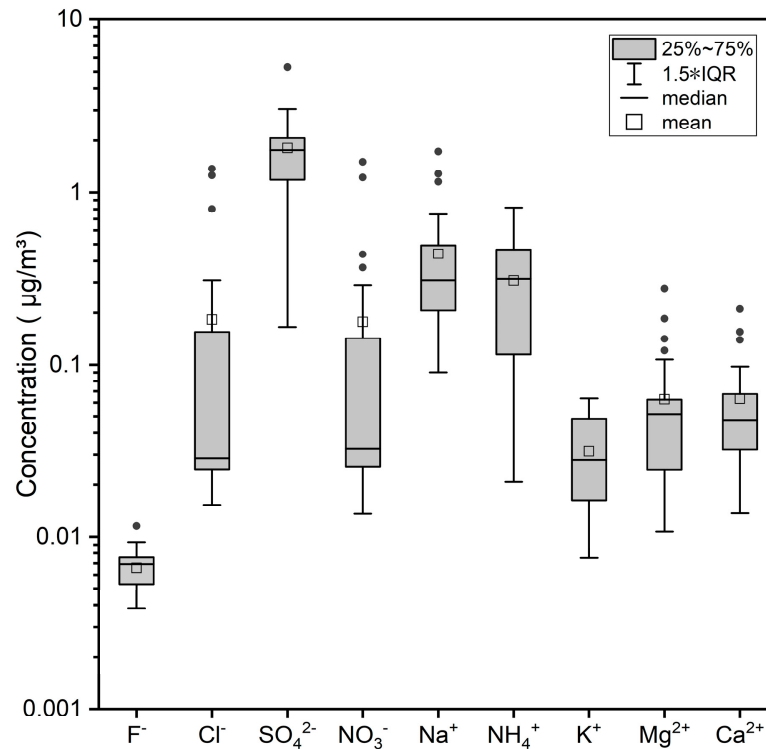


Figure 3. Mass concentrations of PM_{2.5} water-soluble ions in the SCS.

Table 1. Mean mass concentrations of PM_{2.5} ions (µg/m³) and isotope values (‰) in the SCS.

		SO ₄ ²⁻	Na ⁺	NH ₄ ⁺	NO ₃ ⁻	Cl ⁻	K ⁺	Mg ²⁺	Ca ²⁺	δ ³⁴ S-SO ₄ ²⁻	δ ¹⁵ N-NO ₃ ⁻	δ ¹⁸ O-NO ₃ ⁻
Easterly winds	Mean	2.13	0.56	0.35	0.28	0.28	0.04	0.08	0.07	9.04	-1.80	54.19
	SD	1.09	0.48	0.25	0.48	0.48	0.01	0.08	0.07	2.20	2.18	7.07
Southwesterly winds	Mean	1.48	0.32	0.26	0.07	0.09	0.02	0.05	0.05	8.36	0.20	50.07
	SD	0.67	0.20	0.18	0.09	0.11	0.02	0.03	0.04	1.21	2.16	7.33
Total	Mean	1.81	0.44	0.31	0.18	0.18	0.03	0.06	0.06	8.71	-0.89	52.32
	SD	0.95	0.38	0.22	0.35	0.36	0.02	0.06	0.05	1.80	2.35	7.32

Backward trajectories showed significant differences over the SCS during the campaign (Figure 4b). The first half of the cruise was mainly influenced by easterly winds. The wind direction then shifted notably towards southwesterly winds in the second half, starting from 22 May, during the outbreak of the summer monsoon in this region. When the easterly winds prevailed and the cruise track was close to the Philippine Islands, the air masses passed through the Philippine Islands, bringing anthropogenic pollutants from the Philippine Islands [35].

When the southwest monsoon prevailed in the second half of the campaign, a significant proportion of air masses passed over the Central South Peninsula (CSP), traveling a longer distance to the sampled cruise and thereby decreasing the influence of continental and anthropogenic pollution. The mean concentrations of all ions during the easterly winds were higher than those during the southwesterly winds (Figure 4a and Table 1), indicating higher concentrations of pollutants from the Philippine archipelago than from the CSP. Further analyses of the pollutant sources will be performed in the next section, specifically focusing on sulfate and nitrate.

3.1.2. Ion Stoichiometric Relationships

The total concentrations of anions and cations were mostly distributed near the slope of 1:1 in Figure 5a, indicating the overall charge balance and the reliability of the ion concentration analysis. The distribution of the Cl⁻/Na⁺ charge concentration was below the slope (1.17) of bulk seawater in Figure 5b, demonstrating significant chloride depletion

(Cl-depletion) in $PM_{2.5}$ during the warm seasons in the SCS. Cl-depletion is common in marine aerosols, primarily caused by the heterogeneous reaction between nitric acid or sulfuric acid and sea salt aerosols under light and acidic conditions [4,36]. These reactions produce volatile hydrogen chloride gas, leading to a lower Cl^-/Na^+ ratio in marine aerosols than in bulk seawater [37].

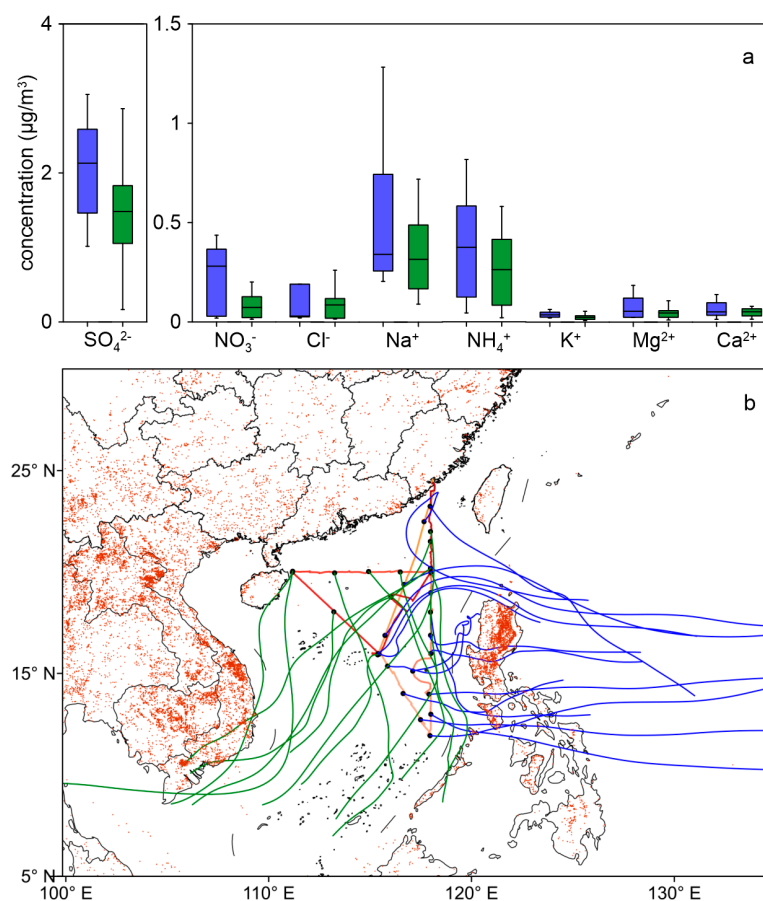


Figure 4. (a) Characteristics of ion concentrations under different prevalent winds in the SCS. The easterly winds are labeled in blue, and southwesterly winds are labeled in green (the lines within the box show the mean value); (b) The 72 h backward trajectories over the SCS during the campaign. The easterly winds are labeled in blue lines, and southwesterly winds are labeled in green lines. The red gradient line from light to dark indicates the cruise route from start to finish. The red solid circles represent the detected fire spots using the MODIS satellite (<https://firms.modaps.eosdis.nasa.gov>, accessed on 9 May 2024), and the map was created using MeteoInfo (version 3.8.11) and Surfer (version 26) software.

The ratio of SO_4^{2-}/Na^+ concentrations was above the slope of bulk seawater (Figure 5c), exhibiting a considerable deviation which suggested a substantial contribution from non-sea-salt sulfate. The ratio of $NH_4^+/nss-SO_4^{2-}$ concentrations was far below the 1:1 slope (Figure 5d), indicating charge disequilibrium between the two ions. However, when the two cations were combined, the ratio of $(Na^+ + NH_4^+)/nss-SO_4^{2-}$ concentrations was close to 1:1 (Figure 5e), indicating charge equilibrium. The above results suggested that sulfuric acid and sodium chloride undergo a permutation reaction, resulting in a significant Cl-depletion in $PM_{2.5}$ in the SCS aerosols, consistent with Hsu et al. (2007) [4]. Our study together with previous studies confirms that sulfate is the primary substitution in the Cl-depletion reaction in fine particles, whereas nitrate is the predominant substitution in the Cl-depletion reaction in coarse particles [4,36].

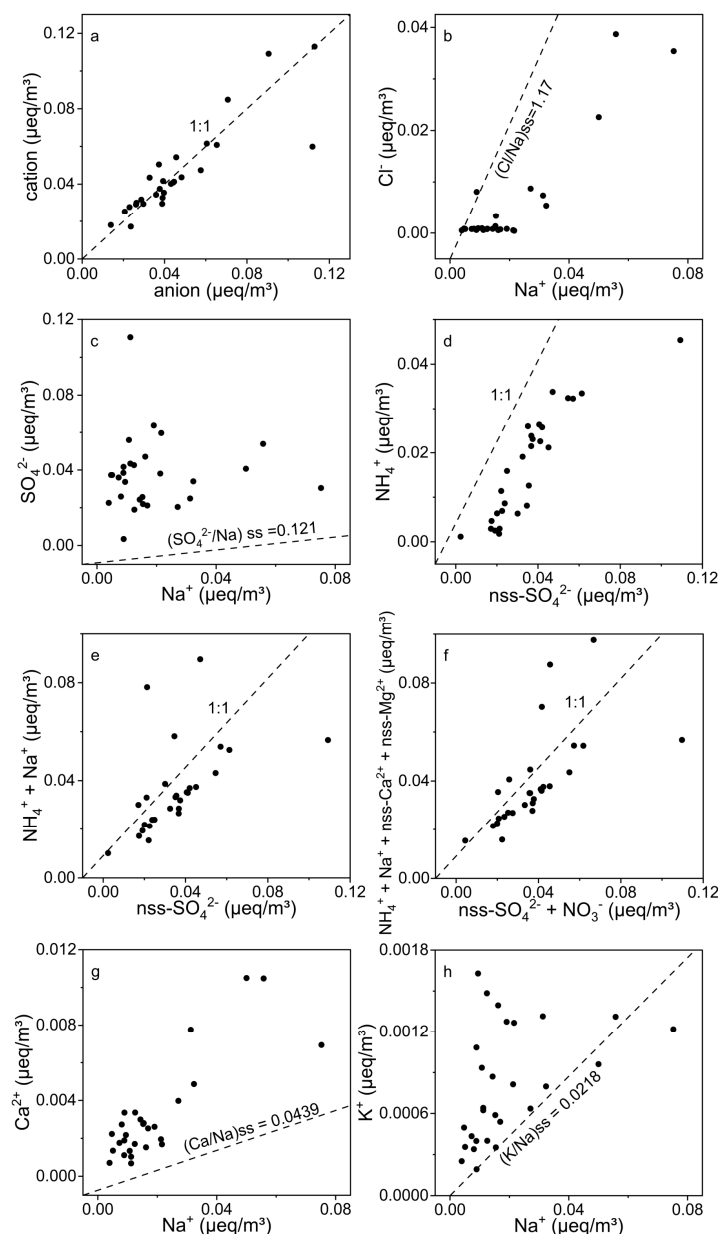


Figure 5. Scatter plots of PM_{2.5} water-soluble ions' stoichiometry in the SCS. (a) The balance between cations and anions with the 1:1 charge ratio; (b) Cl[−] vs. Na⁺, with the seawater ratio of 1.17; (c) SO₄^{2−} vs. Na⁺, with the seawater ratio of 0.121; (d) NH₄⁺ vs. nss-SO₄^{2−}, with the 1:1 stoichiometric relationship; (e) Correlates NH₄⁺ + Na⁺ with nss-SO₄^{2−}; (f) Correlates multiple ions (NH₄⁺ + Na⁺ + nss-Ca²⁺ + nss-Mg²⁺) with nss-SO₄^{2−} + NO₃[−]; (g) Ca²⁺ vs. Na⁺, with the seawater ratio of 0.0439; (h) K⁺ vs. Na⁺, with the seawater ratio of 0.0218.

Overall, the main cations (NH₄⁺ + Na⁺ + nss-Ca²⁺ + nss-Mg²⁺) are balanced by the two main anions (nss-SO₄^{2−} + NO₃[−]) in charge concentrations (Figure 5f). Interestingly, a notable correlation was observed between NO₃[−] and the alkaline earth metal ions Ca²⁺ and Mg²⁺ (Figure S1), suggesting that nitric acid may have undergone a heterogeneous reaction with calcium and magnesium [10]. The concentrations of Ca²⁺ and K⁺ relative to that of Na⁺ were higher than those in bulk seawater (Figure 5g,h), indicating that mineral and biomass burning may be potential sources of Ca²⁺ and K⁺ in addition to sea salt contributions in the SCS. Furthermore, the backward trajectories that intersected land areas with fire hotspots imply the contribution of biomass burning to atmospheric pollutants in the SCS (Figure 4b).

3.2. Composition and Sources of Sulfate Isotopes

3.2.1. Composition of Sulfate Isotopes

Our results agree with previous findings in the marginal seas [13] showing that $\delta^{34}\text{S-SO}_4^{2-}$ values ($8.7 \pm 1.8\%$) are generally lower than those in the polar zones and open oceans but higher than those in inland and coastal cities (Figure 6 and Table S1). When analyzed on a spatial scale, there is a gradual decrease in $\delta^{34}\text{S-SO}_4^{2-}$ values from polar zones and open oceans, to marginal seas, coastal cities, and inland cities of China (Figure 6 and Table S1). This trend in the spatial variation in $\delta^{34}\text{S-SO}_4^{2-}$ values can be attributed to the differences in the sources of sulfate aerosols. The northern and southern polar zones and open oceans, significantly affected by marine biogenic sulfur (mostly DMS) and sea salt, exhibit high aerosol $\delta^{34}\text{S-SO}_4^{2-}$ values, with mean values of 14–18.5‰ [7,38,39] and 10.5–15.7‰ [13,40,41], respectively. However, the $\delta^{34}\text{S}$ values in the polar zones were still slightly lower than those of the sea salt and DMS, suggesting the potential continental transport of sulfate to these regions [7,38].

In contrast, even though coastal cities were next to the ocean, the $\delta^{34}\text{S-SO}_4^{2-}$ mean values of $\text{PM}_{2.5}$ in those cities were typically 5.7–8.9‰ [42–44], much lower than those of the marginal seas, due to increased contributions from fossil fuel combustion. Compared to the coastal cities, the $\delta^{34}\text{S-SO}_4^{2-}$ variations in inland cities were mainly affected by fossil fuel combustion. The $\delta^{34}\text{S-SO}_4^{2-}$ composition of aerosols in most inland cities in China is related to local fossil fuel combustion, such as coal and gasoline combustion. For example, the mean $\delta^{34}\text{S-SO}_4^{2-}$ values were 0.8–7.5‰ in northern cities, which were higher than the values of 0.2–5.7‰ in southern cities in China, due to higher $\delta^{34}\text{S}$ values of coal in northern China [14].

However, in the marginal seas, including the SCS observed in this study and the Sea of Japan [13], the $\delta^{34}\text{S-SO}_4^{2-}$ values (8.7–13.2‰) were generally lower than those in the polar zones and open oceans but higher than those in inland and coastal cities. These results indicated that the combined influence of oceanic and inland air masses on marginal seas from both biogenic sources and combustion sources were significant (i.e., the results from this study and those of Inomata et al. (2019) [13]).

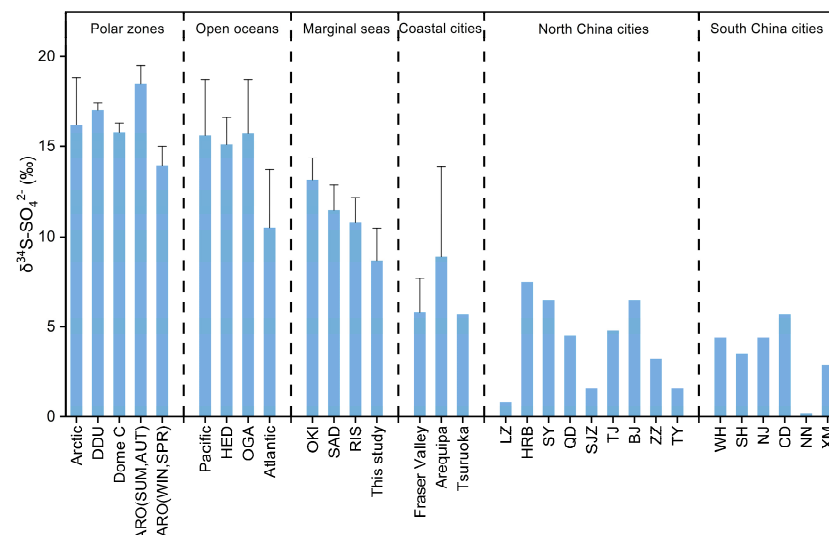


Figure 6. Spatial variation in $\delta^{34}\text{S-SO}_4^{2-}$ values in aerosols from different geographical regions across the globe. The bar graphs indicate the mean value, and the whiskers indicate the standard deviation. Data on Arctic from Ghahreman et al. (2016) [38]; Data on DDU and Dome C from Ishino et al. (2019) [39]; Data on ARO from Walters et al. (2019) [7]; Data on Pacific from Calhoun et al. (1991) [41]; Data on HED, OGA, OKI, SAD, and RIS from Inomata et al. (2019) [13]; Data on Atlantic from Lin et al. (2012) [40]; Data on Fraser Valley from Norman et al. (2006) [42]; Data on Arequipa from Olson et al. (2021) [44]; Data on Tsuruoka from Akata et al. (2010) [43]; and Data on North and South China cities from Wang et al. (2021) [14].

The employed isotopic approach identifies the source origins of atmospheric sulfate based on the distinct $\delta^{34}\text{S}$ values of aerosols. Natural sources primarily include sea salt, DMS (dimethyl sulfide), and microbial emissions, while anthropogenic and continental sources are mainly related to fossil fuel combustion (coal combustion, vehicle exhaust, gas combustion, and ship emissions) and biomass burning. According to previous studies, there are significant differences in the distribution of sulfur isotope values from various sources (Figure 7). Notably, the sulfur isotope values for sea-salt sulfate (20.2–22.1‰) and DMS (18.9–20.3‰) are the highest, with these two sources exhibiting very similar isotope values [17,18]. Therefore, it is challenging to distinguish between these sources using isotope approaches alone. Compared to sea-salt sulfate and DMS, biomass burning has lower sulfur isotope values (4.2–7.9‰) [20,22], followed by fossil fuel combustion (−2.88–10‰) [19–21]. Among the sources listed in Figure 7, microbial emissions exhibit the lowest sulfur isotope values (−28–−15‰) [45].

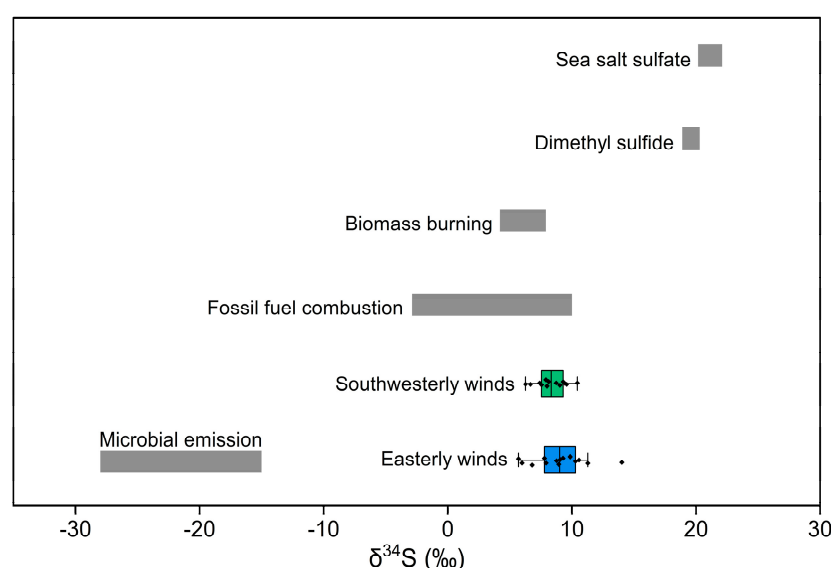


Figure 7. Variations in $\delta^{34}\text{S}$ values for sulfur sources and $\delta^{34}\text{S}\text{-SO}_4^{2-}$ values under different prevalent winds in the SCS (lines within the box show the mean value).

Additionally, the sulfate isotope values during the prevalence of easterly winds (5.7–14.1‰) and southwesterly winds (6.3–10.5‰) were similar. A p -value test showed no significant difference ($p = 0.335 > 0.01$), indicating that the sources of SCS sulfate were similar under both wind directions. Therefore, the isotopic approach to sulfate source resolution for different wind directions is not further discussed. The results of this study showed that under the prevailing easterly and southwesterly winds, the $\delta^{34}\text{S}\text{-SO}_4^{2-}$ values of SCS sulfate were positioned between the values for sea salt, DMS, and marine microbes and were close to the $\delta^{34}\text{S}$ values of sulfur sources from biomass burning and fossil fuel combustion (Figure 7). This suggested that the source of SCS sulfate was not solely influenced by oceanic sources.

3.2.2. Source Apportionment of Sulfate

The sulfur isotopic approach apportions sources based on changes in isotopic composition from emission sources to aerosol sulfate isotopes. The oxidation process of SO_2 (heterogeneous or homogeneous) involves isotopic fractionation, leading to differences in SO_2 and sulfate isotope values [46,47]. Therefore, isotopic fractionation factors (ϵ) are essential for accurately resolving sources using isotopic methods. In this study, fractionation factors could not be calculated due to the lack of observed SO_2 isotope values. As a result, this study analyzed the potential sources of sulfate in the SCS using the SIAR model based on the reported sulfur fractionation factors (−1 to 3‰) in summer from previous studies [46,48].

The results showed that sea salt and DMS contributed between 32 and 48% to sulfate when the fractionation factors ranged from -1 to 3 ‰ (Figure 8). The contribution of $ss\text{-SO}_4^{2-}$ was calculated at 9.0% using the formula $ss\text{-SO}_4^{2-} = 0.252 * [\text{Na}^+]$, suggesting the significant contribution of DMS to the SCS sulfate. The influence of DMS on marine aerosols has been reported on remote islands in the North Pacific Ocean [13]. Furthermore, combustion sources (fossil fuel and biomass; see Figure 8) contribute about 50% to sulfate. Backward trajectory analyses revealed that the air masses passed over land with a high density of fires in Southeast Asia (Figure 4b). Therefore, emissions from fire combustion were potentially important sources of sulfate in the SCS [35,49]. Additionally, microbial emissions contributed approximately 13% to sulfate, indicating that they are non-negligible contributors.

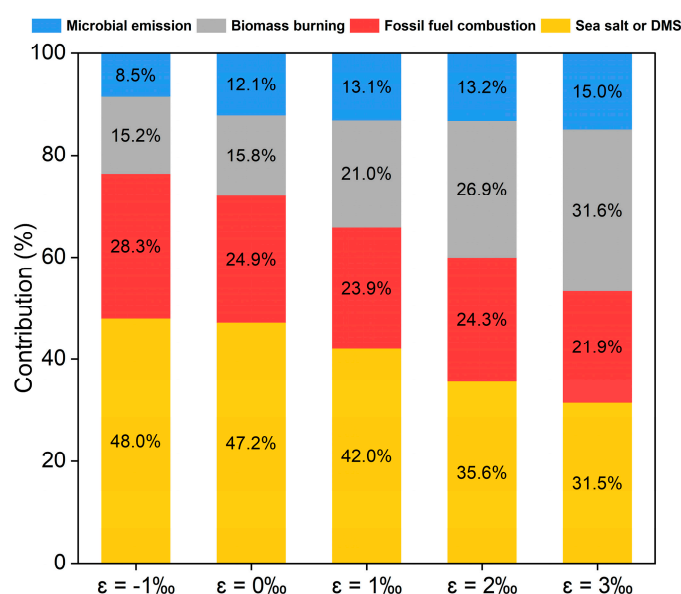


Figure 8. Effect of the fractionation factor (ϵ) on the source contribution to sulfate.

Our results align with observations that the SCS is influenced by both anthropogenic sources, such as fossil fuel combustion and biomass burning, and natural emissions, mostly DMS. Overall, we conclude that the fractionation factor plays a crucial role in the distribution of contributions among different sources. It is essential to account for the fractionation effect when employing isotopic methods to resolve source contributions.

3.3. Composition and Sources of Nitrate Isotopes

3.3.1. Composition of Nitrate Isotopes

Our results concur with previous findings in the SCS [16,50], demonstrating that NO_3^- concentration ($0.2 \pm 0.4 \mu\text{g}/\text{m}^3$), $\delta^{15}\text{N}\text{-NO}_3^-$ (-0.9 ± 2.4 ‰), and $\delta^{18}\text{O}\text{-NO}_3^-$ (52.3 ± 7.3 ‰) values are generally lower than in inland and other coastal areas, yet higher than those in low-latitude open-ocean regions (Table S2). To enhance the understanding of the sources and formation pathways of nitrate, this study summarized the isotopic signatures of the spatial and temporal distribution of nitrate based on our research and previous reports (Table S2). Overall, the NO_3^- concentration and $\delta^{15}\text{N}$ values are primarily influenced by source origins and regional transport, while $\delta^{18}\text{O}$ is more closely associated with the secondary formation [51–53]. Temporally, the NO_3^- concentration, $\delta^{15}\text{N}$ value, and $\delta^{18}\text{O}$ value are higher in the winter or cold seasons compared to the summer or warm seasons. This trend could be attributed to higher emissions from coal combustion ($\delta^{15}\text{N}\text{-NO}_x$, 11.2–18.6‰) in winter [24,26], leading to higher concentrations of NO_3^- and $\delta^{15}\text{N}$. Moreover, stagnant atmospheric conditions in winter impede pollutant dispersion, leading to elevated NO_3^- concentrations [15,32,54,55]. For $\delta^{18}\text{O}$, reduced solar radiation in winter

diminishes the $\text{NO}_2 + \bullet\text{OH}$ reaction but enhances heterogeneous N_2O_5 uptake, resulting in higher $\delta^{18}\text{O}$ levels [55,56].

The extensive spatial variability of NO_x emissions, regional transport, and formation mechanisms across East Asia and the surrounding marine regions ($0\text{--}50^\circ \text{E}$) also contributes to the heterogeneity of NO_3^- characteristics. Our findings indicated a gradual decrease in NO_3^- concentration and $\delta^{15}\text{N}$ values from inland and coastal cities to islands, marginal seas, and the open ocean. This trend signified the typical spatial variation in NO_3^- from emission source regions to transition regions and ultimately to pollution sink regions. In inland and coastal cities, dense populations and industrial activities lead to significant anthropogenic NO_x emissions, particularly from fossil fuel combustion [57], resulting in severe NO_3^- pollution and high $\delta^{15}\text{N}$ values. In contrast, islands and marginal seas have attenuated anthropogenic emissions and are more influenced by monsoon transport [58]. In open-ocean regions, where anthropogenic influence is minimal, NO_x emissions primarily originate from ship emissions ($-18.5 \pm 10.9\text{‰}$) [59], leading to low NO_3^- concentrations and $\delta^{15}\text{N}$ values. In comparison, the spatial variability of $\delta^{18}\text{O}$ is more complex. During winter, $\delta^{18}\text{O}$ values decrease significantly with lower latitudes due to increased solar radiation intensity from north to south, enhancing the photolytic production of $\bullet\text{OH}$ from O_3 and making the $\text{NO}_2 + \bullet\text{OH}$ reaction more prominent. Furthermore, severe atmospheric pollution in inland regions during winter provides more reactive surfaces for the N_2O_5 heterogeneous reaction, resulting in higher $\delta^{18}\text{O}$ values in heavily polluted inland cities than in coastal cities and marine regions [32,60].

In addition, the $\delta^{15}\text{N}\text{-NO}_3^-$ values ($-5.6\text{--}2.8\text{‰}$) during the prevalent easterly winds were slightly lower than those ($-1.6\text{--}5.6\text{‰}$) during southwesterly winds (Figure 9a). A p -value test showed no significant difference ($p = 0.043 > 0.01$), indicating that the nitrate was influenced by similar sources under both wind directions in the SCS. In contrast, the $\delta^{18}\text{O}\text{-NO}_3^-$ values ($41.1\text{--}66\text{‰}$) during the prevalent easterly winds were slightly higher than those ($41.1\text{--}61.9\text{‰}$) during southwesterly winds (Figure 9b). Similarly, a p -value test showed no significant difference ($p = 0.196 > 0.01$), indicating that the nitrate formation followed similar pathways under both wind directions in the SCS.

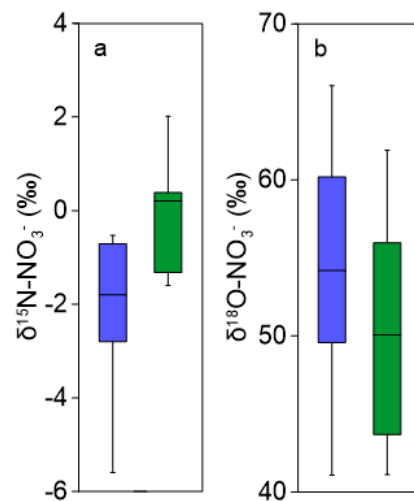


Figure 9. The $\delta^{15}\text{N}\text{-NO}_3^-$ (a) and $\delta^{18}\text{O}\text{-NO}_3^-$ (b) values under different prevalent winds in the SCS. The easterly winds are labeled in blue, and southwesterly winds are labeled in green. The lines within the box show the mean value.

3.3.2. Nitrate Formation Pathways

NO_x is oxidized to nitrate through various atmospheric pathways, each yielding distinct oxygen isotope values due to the different oxidants [61]. The $\delta^{18}\text{O}\text{-HNO}_3$ values for different pathways can be estimated using the calculation methods described by Walters and Michalski (2016) and Michalski et al. (2012) [61,62]. In this study, $\delta^{18}\text{O}\text{-HNO}_3$ values were estimated at $40.1\text{--}55.3\text{‰}$ for the $\text{NO}_2 + \bullet\text{OH}$ pathway, $84.7\text{--}100.6\text{‰}$

for the $\text{N}_2\text{O}_5 + \text{H}_2\text{O}$ pathway, and 83.8–102.9‰ for the $\text{NO}_3 + \text{VOCs}$ pathway in the SCS. Since the SCS is a typical marine environment, nitrate formation involving halogen cannot be neglected [63,64], and $\delta^{18}\text{O}\text{-HNO}_3$ values of 102.2–121.3‰ were estimated for the $\text{N}_2\text{O}_5 + \text{Cl}^-$ pathway (Figure 10a). The $\delta^{18}\text{O}\text{-NO}_3^-$ values during easterly (41.1–66‰) and southwesterly winds (41.1–61.9‰) were close to those of the OH pathway, indicating that the $\text{NO}_2 + \bullet\text{OH}$ reaction was the primary contributor to nitrate in the SCS (Figure 10a).

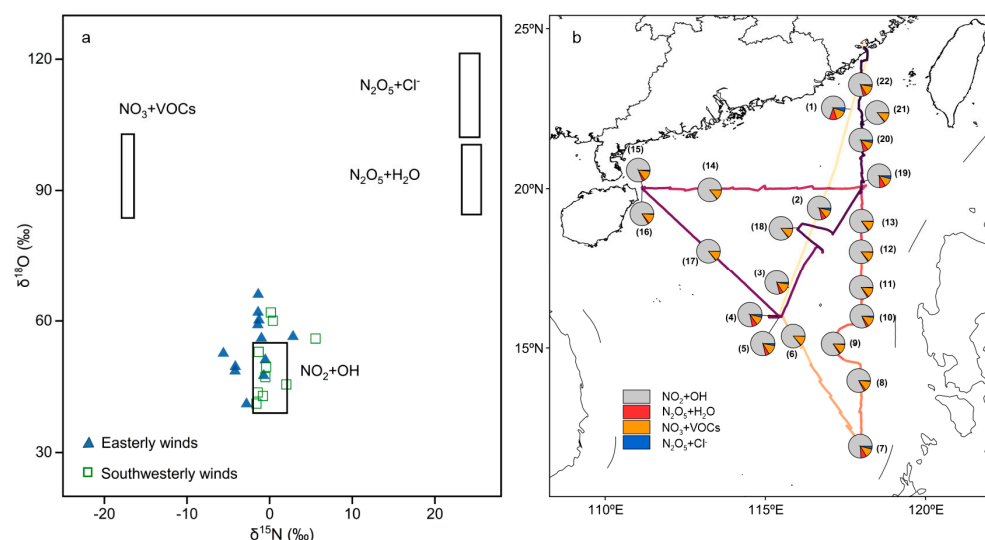


Figure 10. (a) Estimated values of $\delta^{18}\text{O}$ versus $\delta^{15}\text{N}$ formed by different pathways; (b) Fractional contributions of different pathways to nitrate in the SCS along the ship's route. The map was created using MeteInfo (version 3.8.11) software.

The contributions of different nitrate formation pathways along the ship route were calculated using the SIAR model (Figure 10b). Overall, nitrate formation in the SCS follows similar pathways under both wind directions. The lower $\delta^{18}\text{O}\text{-NO}_3^-$ values in the SCS during the summer ($52.3 \pm 7.3\text{‰}$), compared to those observed in the SCS during the summer of 2015 ($65.6 \pm 12.1\text{‰}$) [16], Dongsha Island ($74.2 \pm 7.8\text{‰}$), and Beijing ($84.8 \pm 12.4\text{‰}$) during the spring [11,34], can be attributed to the strong influence of latitude and solar radiation. The $\text{NO}_2 + \bullet\text{OH}$ reaction accounted for 69.8–85.7% of the NO_3^- , which was slightly more than the contribution of Dongsha Island (also located in the SCS) during the spring (56.7–80.2%) [11] and much more than the contribution for Beijing during the spring (45–62%) [34]. This can be attributed to the abundance of $\bullet\text{OH}$ radicals, which are significantly affected by solar radiation [64]. The study region in the SCS, being at a lower latitude than Dongsha Island, particularly during summer, experiences slightly higher levels of solar radiation and temperatures than Dongsha Island and significantly higher levels than Beijing during the spring (around 40°N) [11,34].

In contrast, prolonged sunlight and higher temperatures promote the degradation of O_3 radicals and N_2O_5 , hindering the $\text{NO}_3 + \text{VOCs}$ reaction and heterogeneous N_2O_5 uptake pathways. The $\text{NO}_3 + \text{VOCs}$ pathway contributed 11.3–15.3% to NO_3^- in the SCS, which was slightly less than the contribution of Dongsha Island (14.0–26.4%) [11] and significantly less than the contribution of Beijing (32–40%) [34]. The contributions of the $\text{N}_2\text{O}_5 + \text{H}_2\text{O}$ pathway and $\text{N}_2\text{O}_5 + \text{Cl}^-$ pathway to NO_3^- in the SCS were 0.6–9.8% and 0.4–5.2%, respectively, which were lower than the contributions of Dongsha Island (3.2–8.3% and 2.7–6.5%, respectively) [11], indicating that both pathways contribute insignificantly to NO_3^- in the SCS.

3.3.3. Source Apportionment of Nitrate

Previous studies have identified distinct $\delta^{15}\text{N}\text{-NO}_x$ values for various sources (Figure 11a). For example, anthropogenic sources mainly include natural gas ($-16.5 \pm 1.7\text{‰}$) [65], ship

emissions ($-18.5 \pm 10.9\%$) [59], vehicle exhaust ($-7 \pm 4.8\%$) [15], biomass burning ($-1.7 \pm 4.7\%$) [23–25], and coal combustion ($18.6 \pm 2.9\%$) [26]. Conversely, natural sources mainly consist of soil emissions ($-28.9 \pm 8.2\%$) [66,67] and lightning (0.5%) [68]. Our results showed that under the prevailing easterly and southwesterly winds, the $\delta^{15}\text{N}\text{-NO}_3^-$ values in the SCS, which were positioned between those of various nitrogen oxide sources, do not differ significantly (Figure 11a), suggesting their similar origins.

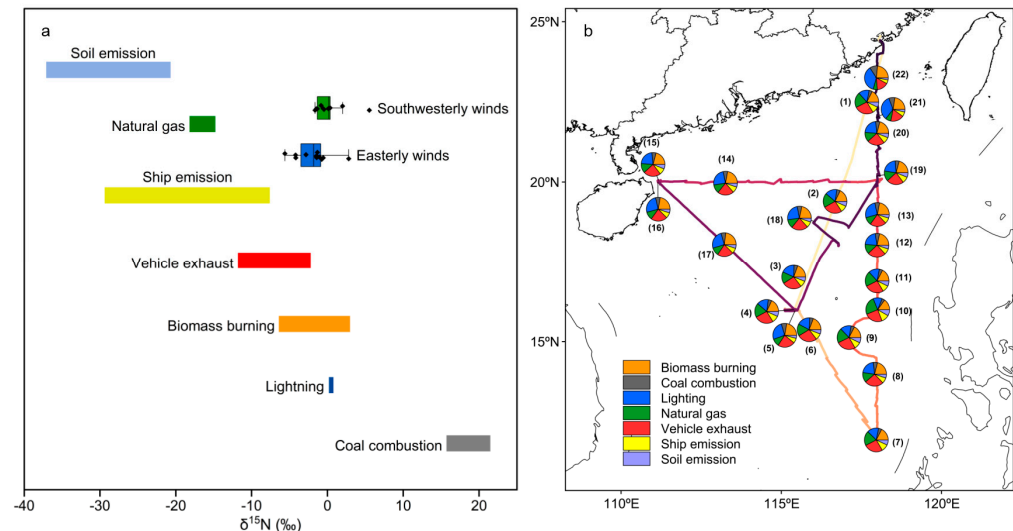


Figure 11. (a) Variations in $\delta^{15}\text{N}$ values for nitrogen sources and $\delta^{15}\text{N}\text{-NO}_3^-$ values under different wind prevalences in the SCS (lines within the box show the mean value); (b) Contributions of sources of nitrate with consideration of fractionation factors (ϵ). Map was created using MeteoInfo (version 3.8.11) software.

The ^{15}N fractionation factor (ϵ) of NO_x during its oxidation to nitrate in the atmosphere can be calculated based on the relative contribution of the nitrate production pathways [69]. The contributions of different emission sources to nitrate in the SCS were estimated using the SIAR model (Figure 11b). The results showed that anthropogenic sources contributed 66.3–80.6%, dominated by vehicle exhaust, biomass burning, and natural gas, with average contributions of 27.1%, 22%, and 14.4%, respectively, and ship emission and coal combustion, with average contributions of 7.1% and 4.3%, respectively. Notably, vehicle exhaust contributes significantly more to nitrate sources than coal combustion. Previous studies indicate that in the regions surrounding the SCS, especially around Guangzhou and urban centers across the China-Indochina Peninsula, vehicle exhaust is a major contributor to nitrate levels [70,71]. Additionally, the contribution of coal combustion to nitrate levels decreases in summer, as coal is not required for heating. In summer, the air masses primarily originating from the SCS result in coal combustion contributing to nitrate at less than half the rate observed during winter in Guangzhou [70].

Biomass burning was identified as one of the primary sources of nitrate during the summer in this study, consistent with other findings conducted in the region [50]. Natural sources contributed 19.4–33.7%, dominated by lightning with an average contribution of 20.6%, and soil emissions with an average contribution of 4.6%. These findings demonstrate that the SCS is affected by both anthropogenic and natural emissions during summer [11,16]. Additionally, no significant differences in the source contributions of nitrate in the SCS were found between the prevailing easterly and southwesterly winds (Figure 11b).

4. Conclusions

The results showed that sulfate accounted for a significantly larger proportion of $\text{PM}_{2.5}$ ions in the SCS compared to other ions, while nitrate was less dominant. Although ionic concentrations were generally higher with prevailing easterly winds than under

southwesterly winds, the sources of sulfate and nitrate remained similar regardless of wind direction. Notably, this research presented the first reported measurements of isotopic values in the SCS during summer. The sulfur isotopic value in sulfate ($\delta^{34}\text{S-SO}_4^{2-}$) was $8.7 \pm 1.8\text{‰}$, while the nitrogen and oxygen isotopic values in nitrate ($\delta^{15}\text{N-NO}_3^-$ and $\delta^{18}\text{O-NO}_3^-$) were $-0.9 \pm 2.4\text{‰}$ and $52.3 \pm 7.3\text{‰}$ in the SCS, respectively.

Our results demonstrated that both natural and anthropogenic sources significantly influenced the aerosol chemistry of this region. The predominant sulfate sources included marine biogenic sulfur (mostly DMS), fossil fuel combustion, and biomass burning, as well as a slight contribution by sea salt. The significant contribution of DMS to sulfate in the SCS also aligns with studies of Walters et al. (2019) [7] and Calhoun et al. (1991) [41] conducted in polar and open-ocean regions, which highlight the important role of DMS in the formation of marine sulfate aerosols. In contrast, nitrate formation was largely governed by the $\text{NO}_2 + \bullet\text{OH}$ pathway (69.8–85.7%) due to the abundance of OH radicals influenced by strong solar radiation, particularly during summer in the lower-latitude SCS. The nitrate was primarily influenced by terrestrial and anthropogenic activities, including vehicle exhaust and biomass burning, along with contributions from natural sources such as lightning. These insights deepen our understanding of atmospheric chemical processes and air quality in the SCS, underscoring that controlling fossil fuel combustion and other anthropogenic activities (e.g., biomass burning) has substantial potential to improve ambient air quality over the SCS. The present study was limited to a single season, and investigating seasonal variations could further expand our understanding of the results. Future research should focus on exploring other seasons to deepen our insights into the aerosol chemistry of the SCS.

Supplementary Materials: The following supporting information can be downloaded at: <https://www.mdpi.com/article/10.3390/su16208733/s1>, Figure S1: Correlation coefficients among major ions of $\text{PM}_{2.5}$ with gaseous pollutants and isotopes; Table S1: Stable sulfur isotopic levels in sulfate aerosols; Table S2: Concentration and stable isotopic levels in nitrate aerosols.

Author Contributions: Y.Z.: conceptualization, methodology, validation, formal analysis, investigation, writing—original draft preparation, writing—review and editing. M.G., X.S., B.L. and C.S.: methodology, formal analysis, investigation, data curation, writing—review and editing. Q.S., X.N., H.O. and S.M.: methodology, validation, formal analysis, investigation, writing—review and editing. S.Z. and J.Z.: conceptualization, methodology, resources, writing—review and editing, supervision, funding acquisition. All authors have read and agreed to the published version of the manuscript.

Funding: This research was funded by National Natural Science Foundation of China (grant numbers 42175115 and 41875152), Innovation Group Project of Southern Marine Science and Engineering Guangdong Laboratory (Zhuhai) (grant numbers 311023001 and 316323005), and the Science and Technology Program of Guangdong Province (Science and Technology Innovation Platform Category, grant number 2019B121201002).

Institutional Review Board Statement: Not applicable.

Informed Consent Statement: Not applicable.

Data Availability Statement: The data are contained within the article and Supplementary Materials.

Conflicts of Interest: The authors declare no conflicts of interest.

References

1. Zhang, R.; Wang, G.; Guo, S.; Zamora, M.L.; Ying, Q.; Lin, Y.; Wang, W.; Hu, M.; Wang, Y. Formation of Urban Fine Particulate Matter. *Chem. Rev.* **2015**, *115*, 3803–3855. [[CrossRef](#)] [[PubMed](#)]
2. Shrivastava, M.; Cappa, C.D.; Fan, J.; Goldstein, A.H.; Guenther, A.B.; Jimenez, J.L.; Kuang, C.; Laskin, A.; Martin, S.T.; Ng, N.L.; et al. Recent Advances in Understanding Secondary Organic Aerosol: Implications for Global Climate Forcing. *Rev. Geophys.* **2017**, *55*, 509–559. [[CrossRef](#)]
3. Qu, Y.; Milliez, M.; Musson-Genon, L.; Carissimo, B. Modelling Radiative and Convective Thermal Exchanges over a European City Center and Their Effects on Atmospheric Dispersion. *Sustainability* **2022**, *14*, 7295. [[CrossRef](#)]

4. Hsu, S.; Liu, S.C.; Kao, S.; Jeng, W.; Huang, Y.; Tseng, C.; Tsai, F.; Tu, J.; Yang, Y. Water-soluble Species in the Marine Aerosol from the Northern South China Sea: High Chloride Depletion Related to Air Pollution. *J. Geophys. Res.* **2007**, *112*, 2007JD008844. [[CrossRef](#)]
5. Zhou, J.; Zhang, J.; Jiang, G.; Xie, K. Using DPF to Control Particulate Matter Emissions from Ships to Ensure the Sustainable Development of the Shipping Industry. *Sustainability* **2024**, *16*, 6642. [[CrossRef](#)]
6. Li, X.; Zhang, R.; Tripathee, L.; Guo, J.; Yang, W.; Guo, J. Influence of Spring Dust Storm on Atmospheric Particulate-Bound Mercury in a Typical Inland City of Northern China: Characteristics, Sources, and Risk Assessment. *Sustainability* **2024**, *16*, 4096. [[CrossRef](#)]
7. Walters, W.W.; Michalski, G.; Böhlke, J.K.; Alexander, B.; Savarino, J.; Thiemens, M.H. Assessing the Seasonal Dynamics of Nitrate and Sulfate Aerosols at the South Pole Utilizing Stable Isotopes. *JGR Atmos.* **2019**, *124*, 8161–8177. [[CrossRef](#)]
8. Elliott, E.M.; Kendall, C.; Wankel, S.D.; Burns, D.A.; Boyer, E.W.; Harlin, K.; Bain, D.J.; Butler, T.J. Nitrogen Isotopes as Indicators of NO_x Source Contributions to Atmospheric Nitrate Deposition Across the Midwestern and Northeastern United States. *Environ. Sci. Technol.* **2007**, *41*, 7661–7667. [[CrossRef](#)]
9. Luo, L.; Wu, S.; Zhang, R.; Wu, Y.; Li, J.; Kao, S. What Controls Aerosol $\delta^{15}\text{N}$ -NO₃⁻? NO_x Emission Sources vs. Nitrogen Isotope Fractionation. *Sci. Total Environ.* **2023**, *871*, 162185. [[CrossRef](#)]
10. Luo, L.; Liao, T.; Zhang, X.; Wu, Y.; Li, J.; Zhang, R.; Zheng, Z.; Kao, S.-J. Quantifying the Formation Pathways of Nitrate in Size-Segregated Aerosols during Winter Haze Pollution. *Gondwana Res.* **2023**, *115*, 71–80. [[CrossRef](#)]
11. Yang, S.; Luo, L.; Li, Y.; Wang, C.; Lu, B.; Xu, S.; Kao, S. Dry deposition fluxes, formation mechanisms and sources of nitrate in total suspended particles in springtime on Dongsha Island, South China Sea. *J. Earth Environ.* **2023**, *14*, 193–206. (In Chinese)
12. Xiao, H.; Zhu, R.; Pan, Y.; Guo, W.; Zheng, N.; Liu, Y.; Liu, C.; Zhang, Z.; Wu, J.; Kang, C.; et al. Differentiation Between Nitrate Aerosol Formation Pathways in a Southeast Chinese City by Dual Isotope and Modeling Studies. *JGR Atmos.* **2020**, *125*, e2020JD032604. [[CrossRef](#)]
13. Inomata, Y.; Ohizumi, T.; Saito, T.; Morohashi, M.; Yamashita, N.; Takahashi, M.; Sase, H.; Takahashi, K.; Kaneyasu, N.; Fujihara, M.; et al. Estimating Transboundary Transported Anthropogenic Sulfate Deposition in Japan Using the Sulfur Isotopic Ratio. *Sci. Total Environ.* **2019**, *691*, 779–788. [[CrossRef](#)]
14. Wang, X.; Li, J.; Sun, R.; Jiang, H.; Zong, Z.; Tian, C.; Xie, L.; Li, Q.; Jia, W.; Peng, P.; et al. Regional Characteristics of Atmospheric $\delta^{34}\text{S}$ -SO₄²⁻ over Three Parts of Asia Monitored by Quartz Wool-Based Passive Samplers. *Sci. Total Environ.* **2021**, *778*, 146107. [[CrossRef](#)] [[PubMed](#)]
15. Zong, Z.; Tan, Y.; Wang, X.; Tian, C.; Li, J.; Fang, Y.; Chen, Y.; Cui, S.; Zhang, G. Dual-Modelling-Based Source Apportionment of NO_x in Five Chinese Megacities: Providing the Isotopic Footprint from 2013 to 2014. *Environ. Int.* **2020**, *137*, 105592. [[CrossRef](#)] [[PubMed](#)]
16. Xiao, H.-W.; Xie, L.-H.; Long, A.-M.; Ye, F.; Pan, Y.-P.; Li, D.-N.; Long, Z.-H.; Chen, L.; Xiao, H.-Y.; Liu, C.-Q. Use of Isotopic Compositions of Nitrate in TSP to Identify Sources and Chemistry in South China Sea. *Atmos. Environ.* **2015**, *109*, 70–78. [[CrossRef](#)]
17. Tostevin, R.; Turchyn, A.V.; Farquhar, J.; Johnston, D.T.; Eldridge, D.L.; Bishop, J.K.B.; McIlvin, M. Multiple Sulfur Isotope Constraints on the Modern Sulfur Cycle. *Earth Planet. Sci. Lett.* **2014**, *396*, 14–21. [[CrossRef](#)]
18. Amrani, A.; Said-Ahmad, W.; Shaked, Y.; Kiene, R.P. Sulfur Isotope Homogeneity of Oceanic DMSP and DMS. *Proc. Natl. Acad. Sci. USA* **2013**, *110*, 18413–18418. [[CrossRef](#)]
19. Rempillo, O.; Seguin, A.M.; Norman, A.-L.; Scarratt, M.; Michaud, S.; Chang, R.; Sjostedt, S.; Abbatt, J.; Else, B.; Papakyriakou, T.; et al. Dimethyl Sulfide Air-Sea Fluxes and Biogenic Sulfur as a Source of New Aerosols in the Arctic Fall. *J. Geophys. Res.* **2011**, *116*, D00S04. [[CrossRef](#)]
20. Xu, Y. Source Analysis of Sulfate in Atmospheric Particulate Matter Based on Sulfur Isotope. Ph.D. Dissertation, North China Electric Power University, Beijing, China, 2023. (In Chinese)
21. Zhang, H.; Hu, A.; Lu, C.; Zhang, G. Sulfur isotopic composition of acid deposition in South China Regions and its environmental significance. *China Environ. Sci.* **2002**, *22*, 165–169. (In Chinese)
22. Guo, Z.; Shi, L.; Chen, S.; Jiang, W.; Wei, Y.; Rui, M.; Zeng, G. Sulfur Isotopic Fractionation and Source Appointment of PM_{2.5} in Nanjing Region around the Second Session of the Youth Olympic Games. *Atmos. Res.* **2016**, *174–175*, 9–17. [[CrossRef](#)]
23. Fibiger, D.L.; Hastings, M.G. First Measurements of the Nitrogen Isotopic Composition of NO_x from Biomass Burning. *Environ. Sci. Technol.* **2016**, *50*, 11569–11574. [[CrossRef](#)] [[PubMed](#)]
24. Zong, Z.; Shi, X.; Sun, Z.; Tian, C.; Li, J.; Fang, Y.; Gao, H.; Zhang, G. Nitrogen Isotopic Composition of NO_x from Residential Biomass Burning and Coal Combustion in North China. *Environ. Pollut.* **2022**, *304*, 119238. [[CrossRef](#)] [[PubMed](#)]
25. Song, W.; Liu, X.-Y. Nitrogen Isotope Signatures of Oxidized Nitrogen Species from Biomass Burning. *Appl. Geochem.* **2023**, *150*, 105569. [[CrossRef](#)]
26. Felix, J.D.; Elliott, E.M.; Shaw, S.L. Nitrogen Isotopic Composition of Coal-Fired Power Plant NO_x: Influence of Emission Controls and Implications for Global Emission Inventories. *Environ. Sci. Technol.* **2012**, *46*, 3528–3535. [[CrossRef](#)]
27. Sigman, D.M.; Casciotti, K.L.; Andreani, M.; Barford, C.; Galanter, M.; Böhlke, J.K. A Bacterial Method for the Nitrogen Isotopic Analysis of Nitrate in Seawater and Freshwater. *Anal. Chem.* **2001**, *73*, 4145–4153. [[CrossRef](#)]
28. Casciotti, K.L.; Sigman, D.M.; Hastings, M.G.; Böhlke, J.K.; Hilkert, A. Measurement of the Oxygen Isotopic Composition of Nitrate in Seawater and Freshwater Using the Denitrifier Method. *Anal. Chem.* **2002**, *74*, 4905–4912. [[CrossRef](#)]

29. Ding, S.; Chen, Y.; Li, Q.; Li, X.-D. Using Stable Sulfur Isotope to Trace Sulfur Oxidation Pathways during the Winter of 2017–2019 in Tianjin, North China. *Int. J. Environ. Res. Public Health* **2022**, *19*, 10966. [[CrossRef](#)]
30. Lin, Y.-C.; Yu, M.; Xie, F.; Zhang, Y. Anthropogenic Emission Sources of Sulfate Aerosols in Hangzhou, East China: Insights from Isotope Techniques with Consideration of Fractionation Effects between Gas-to-Particle Transformations. *Environ. Sci. Technol.* **2022**, *56*, 3905–3914. [[CrossRef](#)]
31. Giesemann, A.; Jaeger, H.-J.; Norman, A.L.; Krouse, H.R.; Brand, W.A. Online Sulfur-Isotope Determination Using an Elemental Analyzer Coupled to a Mass Spectrometer. *Anal. Chem.* **1994**, *66*, 2816–2819. [[CrossRef](#)]
32. Luo, L.; Zhu, R.; Song, C.-B.; Peng, J.-F.; Guo, W.; Liu, Y.; Zheng, N.; Xiao, H.; Xiao, H.-Y. Changes in Nitrate Accumulation Mechanisms as PM_{2.5} Levels Increase on the North China Plain: A Perspective from the Dual Isotopic Compositions of Nitrate. *Chemosphere* **2021**, *263*, 127915. [[CrossRef](#)]
33. Parnell, A.C.; Phillips, D.L.; Bearhop, S.; Semmens, B.X.; Ward, E.J.; Moore, J.W.; Jackson, A.L.; Grey, J.; Kelly, D.J.; Inger, R. Bayesian Stable Isotope Mixing Models. *Environmetrics* **2013**, *24*, 387–399. [[CrossRef](#)]
34. Luo, L.; Kao, S.; Wu, Y.; Zhang, X.; Lin, H.; Zhang, R.; Xiao, H. Stable Oxygen Isotope Constraints on Nitrate Formation in Beijing in Springtime. *Environ. Pollut.* **2020**, *263*, 114515. [[CrossRef](#)] [[PubMed](#)]
35. Saksakulkrai, S.; Chantara, S.; Shi, Z. Airborne Particulate Matter in Southeast Asia: A Review on Variation, Chemical Compositions and Source Apportionment. *Environ. Chem.* **2023**, *19*, 401–431. [[CrossRef](#)]
36. Yao, X.; Zhang, L. Chemical Processes in Sea-Salt Chloride Depletion Observed at a Canadian Rural Coastal Site. *Atmos. Environ.* **2012**, *46*, 189–194. [[CrossRef](#)]
37. Sturges, W.T.; Shaw, G.E. Halogens in Aerosols in Central Alaska. *Atmos. Environ. Part A. Gen. Top.* **1993**, *27*, 2969–2977. [[CrossRef](#)]
38. Ghahreman, R.; Norman, A.-L.; Abbatt, J.P.D.; Lévassieur, M.; Thomas, J.L. Biogenic, Anthropogenic and Sea Salt Sulfate Size-Segregated Aerosols in the Arctic Summer. *Atmos. Chem. Phys.* **2016**, *16*, 5191–5202. [[CrossRef](#)]
39. Ishino, S.; Hattori, S.; Savarino, J.; Legrand, M.; Albalat, E.; Albaredo, F.; Preunkert, S.; Jourdain, B.; Yoshida, N. Homogeneous Sulfur Isotope Signature in East Antarctica and Implication for Sulfur Source Shifts through the Last Glacial-Interglacial Cycle. *Sci. Rep.* **2019**, *9*, 12378. [[CrossRef](#)]
40. Lin, C.T.; Baker, A.R.; Jickells, T.D.; Kelly, S.; Lesworth, T. An Assessment of the Significance of Sulphate Sources over the Atlantic Ocean Based on Sulphur Isotope Data. *Atmos. Environ.* **2012**, *62*, 615–621. [[CrossRef](#)]
41. Calhoun, J.A.; Bates, T.S.; Charlson, R.J. Sulfur Isotope Measurements of Submicrometer Sulfate Aerosol Particles over the Pacific Ocean. *Geophys. Res. Lett.* **1991**, *18*, 1877–1880. [[CrossRef](#)]
42. Norman, A.-L.; Anlauf, K.; Hayden, K.; Thompson, B.; Brook, J.R.; Li, S.-M.; Bottenheim, J. Aerosol Sulphate and Its Oxidation on the Pacific NW Coast: S and O Isotopes in PM_{2.5}. *Atmos. Environ.* **2006**, *40*, 2676–2689. [[CrossRef](#)]
43. Akata, N.; Yanagisawa, F.; Kotani, T.; Ueda, A. Ten-Year Observation of Sulfur Isotopic Composition of Sulfate in Aerosols Collected at Tsuruoka, a Coastal Area on the Sea of Japan in Northern Japan. *Geochem. J.* **2010**, *44*, 571–577. [[CrossRef](#)]
44. Olson, E.; Michalski, G.; Welp, L.; Larrea Valdivia, A.E.; Reyes Larico, J.; Salcedo Peña, J.; Fang, H.; Magara Gomez, K.; Li, J. Mineral Dust and Fossil Fuel Combustion Dominate Sources of Aerosol Sulfate in Urban Peru Identified by Sulfur Stable Isotopes and Water-Soluble Ions. *Atmos. Environ.* **2021**, *260*, 118482. [[CrossRef](#)]
45. Rabinovich, A.L.; Grinenko, V.A. Sulfate Sulfur Isotope Ratios for USSR River Water. *Geochem. Int.* **1979**, *16*, 68–79.
46. Mukai, H.; Tanaka, A.; Fujii, T.; Zeng, Y.; Hong, Y.; Tang, J.; Guo, S.; Xue, H.; Sun, Z.; Zhou, J.; et al. Regional Characteristics of Sulfur and Lead Isotope Ratios in the Atmosphere at Several Chinese Urban Sites. *Environ. Sci. Technol.* **2001**, *35*, 1064–1071. [[CrossRef](#)]
47. Guo, Z.; Guo, Q.; Chen, S.; Zhu, B.; Zhang, Y.; Yu, J.; Guo, Z. Study on Pollution Behavior and Sulfate Formation during the Typical Haze Event in Nanjing with Water Soluble Inorganic Ions and Sulfur Isotopes. *Atmos. Res.* **2019**, *217*, 198–207. [[CrossRef](#)]
48. Han, X.; Lang, Y.; Guo, Q.; Li, X.; Ding, H.; Li, S. Enhanced Oxidation of SO₂ by H₂O₂ during Haze Events: Constraints From Sulfur Isotopes. *JGR Atmos.* **2022**, *127*, e2022JD036960. [[CrossRef](#)]
49. Xiao, H.-W.; Xiao, H.-Y.; Luo, L.; Shen, C.-Y.; Long, A.-M.; Chen, L.; Long, Z.-H.; Li, D.-N. Atmospheric Aerosol Compositions over the South China Sea: Temporal Variability and Source Apportionment. *Atmos. Chem. Phys.* **2017**, *17*, 3199–3214. [[CrossRef](#)]
50. Yang, J.-Y.T.; Hsu, S.-C.; Dai, M.H.; Hsiao, S.S.-Y.; Kao, S.-J. Isotopic Composition of Water-Soluble Nitrate in Bulk Atmospheric Deposition at Dongsha Island: Sources and Implications of External N Supply to the Northern South China Sea. *Biogeosciences* **2014**, *11*, 1833–1846. [[CrossRef](#)]
51. Altieri, K.E.; Fawcett, S.E.; Hastings, M.G. Reactive Nitrogen Cycling in the Atmosphere and Ocean. *Annu. Rev. Earth Planet. Sci.* **2021**, *49*, 523–550. [[CrossRef](#)]
52. Zhen, S.; Luo, M.; Shao, Y.; Xu, D.; Ma, L. Application of Stable Isotope Techniques in Tracing the Sources of Atmospheric NO_x and Nitrate. *Processes* **2022**, *10*, 2549. [[CrossRef](#)]
53. Chen, M.; Niu, H.; Xiang, Y. A Study of Chemical Processes of Nitrate in Atmospheric Aerosol and Snow Based on Stable Isotopes. *Atmosphere* **2023**, *15*, 59. [[CrossRef](#)]
54. Zhang, W.; Wu, F.; Luo, X.; Song, L.; Wang, X.; Zhang, Y.; Wu, J.; Xiao, Z.; Cao, F.; Bi, X.; et al. Quantification of NO Sources Contribution to Ambient Nitrate Aerosol, Uncertainty Analysis and Sensitivity Analysis in a Megacity. *Sci. Total Environ.* **2024**, *926*, 171583. [[CrossRef](#)] [[PubMed](#)]

55. Huang, W.; Ye, X.; Lv, Z.; Yao, Y.; Chen, Y.; Zhou, Y.; Chen, J. Dual Isotopic Evidence of $\delta^{15}\text{N}$ and $\delta^{18}\text{O}$ for Priority Control of Vehicle Emissions in a Megacity of East China: Insight from Measurements in Summer and Winter. *Sci. Total Environ.* **2024**, *931*, 172918. [[CrossRef](#)] [[PubMed](#)]
56. Liu, L.; Bei, N.; Hu, B.; Wu, J.; Liu, S.; Li, X.; Wang, R.; Liu, Z.; Shen, Z.; Li, G. Wintertime Nitrate Formation Pathways in the North China Plain: Importance of N_2O_5 Heterogeneous Hydrolysis. *Environ. Pollut.* **2020**, *266*, 115287. [[CrossRef](#)] [[PubMed](#)]
57. Han, S.; Huang, W.; Cui, S.; Gao, B.; Zhai, Y. Productive and Consumptive Emission Characteristics of Energy-Related Nitrogen Oxides in Eastern Chinese Cities. *Ecosyst. Health Sustain.* **2024**, *10*, 0226. [[CrossRef](#)]
58. Reid, J.S.; Lagrosas, N.D.; Jonsson, H.H.; Reid, E.A.; Sessions, W.R.; Simpas, J.B.; Uy, S.N.; Boyd, T.J.; Atwood, S.A.; Blake, D.R.; et al. Observations of the Temporal Variability in Aerosol Properties and Their Relationships to Meteorology in the Summer Monsoonal South China Sea/East Sea: The Scale-Dependent Role of Monsoonal Flows, the Madden–Julian Oscillation, Tropical Cyclones, Squall Lines and Cold Pools. *Atmos. Chem. Phys.* **2015**, *15*, 1745–1768. [[CrossRef](#)]
59. Sun, Z.; Zong, Z.; Tan, Y.; Tian, C.; Liu, Z.; Zhang, F.; Sun, R.; Chen, Y.; Li, J.; Zhang, G. Characterization of the Nitrogen Stable Isotope Composition ($\delta^{15}\text{N}$) of Ship-Emitted NO_x . *Atmos. Chem. Phys.* **2023**, *23*, 12851–12865. [[CrossRef](#)]
60. Deng, M.; Wang, C.; Yang, C.; Li, X.; Cheng, H. Nitrogen and Oxygen Isotope Characteristics, Formation Mechanism, and Source Apportionment of Nitrate Aerosols in Wuhan, Central China. *Sci. Total Environ.* **2024**, *921*, 170715. [[CrossRef](#)]
61. Michalski, G.; Bhattacharya, S.K.; Mase, D.F. Oxygen Isotope Dynamics of Atmospheric Nitrate and Its Precursor Molecules. In *Handbook of Environmental Isotope Geochemistry: Vol I*; Baskaran, M., Ed.; Springer: Berlin/Heidelberg, Germany, 2012; pp. 613–635. ISBN 978-3-642-10637-8.
62. Walters, W.W.; Michalski, G. Theoretical Calculation of Oxygen Equilibrium Isotope Fractionation Factors Involving Various NO Molecules, OH , and H_2O and Its Implications for Isotope Variations in Atmospheric Nitrate. *Geochim. Cosmochim. Acta* **2016**, *191*, 89–101. [[CrossRef](#)]
63. Stark, H.; Brown, S.S.; Goldan, P.D.; Aldener, M.; Kuster, W.C.; Jakoubek, R.; Fehsenfeld, F.C.; Meagher, J.; Bates, T.S.; Ravishankara, A.R. Influence of Nitrate Radical on the Oxidation of Dimethyl Sulfide in a Polluted Marine Environment. *J. Geophys. Res.* **2007**, *112*, 2006JD007669. [[CrossRef](#)]
64. Kamezaki, K.; Hattori, S.; Iwamoto, Y.; Ishino, S.; Furutani, H.; Miki, Y.; Uematsu, M.; Miura, K.; Yoshida, N. Tracing the Sources and Formation Pathways of Atmospheric Particulate Nitrate over the Pacific Ocean Using Stable Isotopes. *Atmos. Environ.* **2019**, *209*, 152–166. [[CrossRef](#)]
65. Walters, W.W.; Tharp, B.D.; Fang, H.; Kozak, B.J.; Michalski, G. Nitrogen Isotope Composition of Thermally Produced NO_x from Various Fossil-Fuel Combustion Sources. *Environ. Sci. Technol.* **2015**, *49*, 11363–11371. [[CrossRef](#)]
66. Li, D.; Wang, X. Nitrogen Isotopic Signature of Soil-Released Nitric Oxide (NO) after Fertilizer Application. *Atmos. Environ.* **2008**, *42*, 4747–4754. [[CrossRef](#)]
67. Felix, J.D.; Elliott, E.M. Isotopic Composition of Passively Collected Nitrogen Dioxide Emissions: Vehicle, Soil and Livestock Source Signatures. *Atmos. Environ.* **2014**, *92*, 359–366. [[CrossRef](#)]
68. Hoering, T. The Isotopic Composition of the Ammonia and the Nitrate Ion in Rain. *Geochim. Cosmochim. Acta* **1957**, *12*, 97–102. [[CrossRef](#)]
69. Walters, W.W.; Michalski, G. Theoretical Calculation of Nitrogen Isotope Equilibrium Exchange Fractionation Factors for Various NO_y Molecules. *Geochim. Cosmochim. Acta* **2015**, *164*, 284–297. [[CrossRef](#)]
70. Li, T.; Li, J.; Sun, Z.; Jiang, H.; Tian, C.; Zhang, G. High Contribution of Anthropogenic Combustion Sources to Atmospheric Inorganic Reactive Nitrogen in South China Evidenced by Isotopes. *Atmos. Chem. Phys.* **2023**, *23*, 6395–6407. [[CrossRef](#)]
71. Wang, X.; Li, J.; Tian, C.; Zong, Z.; Liu, Q.; Jiang, H.; Li, T.; Li, J.; Jiang, H.; Zhao, S.; et al. Sources and Formation of Atmospheric Nitrate Over China–Indochina Peninsula in Spring: A Perspective From Oxygen and Nitrogen Isotopic Compositions Based on Passive Air Samplers. *Front. Environ. Sci.* **2022**, *10*, 897555. [[CrossRef](#)]

Disclaimer/Publisher’s Note: The statements, opinions and data contained in all publications are solely those of the individual author(s) and contributor(s) and not of MDPI and/or the editor(s). MDPI and/or the editor(s) disclaim responsibility for any injury to people or property resulting from any ideas, methods, instructions or products referred to in the content.